Relationship between the Local Electronic and Local Crystal Structures of Intermediate-Valence $Sm_{1-x}Y_xS$

A. P. Menushenkov[a], R. V. Chernikov[a], V. V. Sidorov[a], K. V. Klementiev[b], P. A. Alekseev[c], and A. V. Rybina[c]

[a] Moscow Engineering Physics Institute (State University), Kashirskoe sh. 31, Moscow, 115409 Russia
e-mail: menushen@htsc.mephi.ru
[b] HASYLAB, DESY, D-22607 Hamburg, Germany
[c] Russian Research Centre Kurchatov Institute, pl. Kurchatova 1, Moscow, 123182 Russia
Received June 6, 2006

The valence state of samarium and the local environments of samarium and yttrium ions in the intermediate-valence compound $Sm_{1-x}Y_xS$ ($x = 0.17$, 0.25, 0.33, or 0.45) are studied over a wide temperature range of 20–300 K using x-ray absorption spectroscopy. The temperature dependence of Sm–S, Sm–Sm(Y), Y–S, and Y−Sm(Y) bond lengths and the Debye–Waller factors has been found. A direct correlation of changes in the valence of samarium with changes in its local environment parameters depending on yttrium concentration and temperature has been revealed. The main characteristics of the intermediate-valence state of samarium have been determined: the energy width of the $4f$ level and its position with respect to the Fermi level.

Samarium sulfide (SmS) belongs to the class of compounds with homogeneous intermediate valence, which is observed in a metal phase at a pressure of ≳0.6 GPa above the point of the dielectric–metal phase transition because of a partial delocalization of the $4f^6$ electron [1]. Upon the transition, the crystal lattice decreased significantly in volume with the retention of the NaCl symmetry. An intermediate-valence state can also be achieved by replacing a portion of samarium ions by other smaller radius rare earth or transition metal ions (Y^{3+}, Yb^{3+}, Gd^{3+}, etc.). It is believed that the resulting chemical contraction serves as an equivalent of external pressure. However, attempts to initiate the dielectric–metal phase transition using chemical contraction upon the insertion of bivalent ions, such as Ca^{2+}, were unsuccessful, although x-ray absorption spectroscopic data indicated the appearance of an intermediate-valence state [2]. This suggests that doping and the resulting chemical contraction inevitably affect the electronic and crystal structures at a local level and thereby change the properties of the intermediate-valence state and the macroscopic properties of the compound.

The recently growing interest in compounds based on samarium sulfide is considerably related to a number of anomalies observed in these compounds, such as a negative coefficient of thermal expansion in the metallic phase of SmS [3] and unusual magnetic properties of the dielectric phase of $Sm_{1-x}Y_xS$ [4]. Thus, the recently found collective magnetic excitations in the inelastic

neutron scattering spectra of $Sm_{0.83}Y_{0.17}S$ [4] have not found an interpretation in terms of the classical model of intermediate valence. They were explained based on the occurrence of a locally bound state by analogy with the model of intermediate valence developed for SmB_6 [5]. At the same time, Fishman and Liu [6] theoretically interpreted the above peculiarities as a result of local lattice symmetry breakdown upon the insertion of an Y^{3+} impurity; moreover, they cast doubt on the occurrence of an intermediate-valence state in $Sm_{1-x}Y_xS$.

Thus, in order to reveal the nature of the intermediate-valence state, determine the role of doping, and explain the macroscopic properties of $Sm_{1-x}Y_xS$, a study of the local electronic and crystal structure peculiarities is brought to the forefront. For this purpose, in this work, we used a combination of x-ray absorption near-edge structure (XANES) and extended x-ray absorption fine structure (EXAFS) techniques, which allowed us to simultaneously study the valence states and local environment parameters of the test ions.

The samples with the yttrium contents $x = 0.17$ and 0.33 were prepared at the Ioffe Physicotechnical Institute, Russian Academy of Sciences (St. Petersburg, Russia), and the samples with $x = 0.25$ and 0.45 were prepared at Tohoku University (Sendai, Japan).

The x-ray absorption spectra of $Sm_{1-x}Y_xS$ ($x = 0.17$, 0.25, 0.33, and 0.45) were measured over the temperature range 20–300 K above the Sm L_{III} and Y K edges at the beamlines $E4$ and $A1$ of the HASYLAB synchrotron center (DESY, Germany). The use of a Si(111)
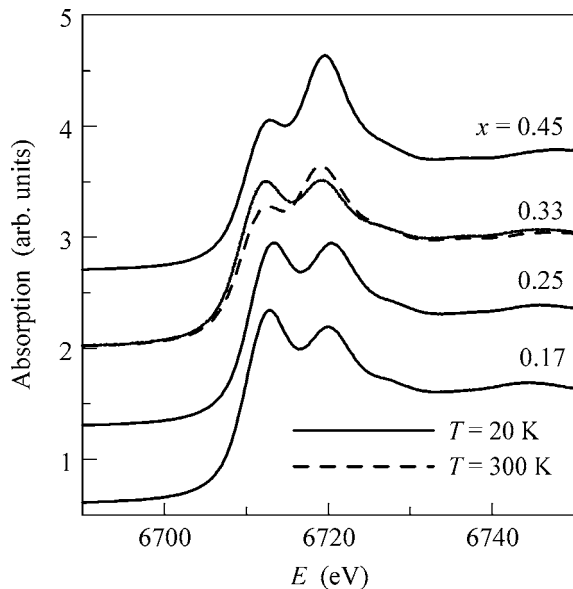
Fig. 1. X-ray absorption spectra of $Sm_{1-x}Y_xS$ near the L_{III} absorption edge of Sm at 20 K. The dashed line shows the absorption spectrum of the composition with $x = 0.33$ at $T = 300$ K.

double crystal ($E4$) or Si(111) channel-cut crystal ($A1$) monochromator gave an energy resolution of ~1.2 or ~2.5 eV at x-radiation energy of 6716 or 17038 eV in the L_{III}-edge region of Sm or the K-edge region of Y, respectively. The low-temperature measurements were performed with a closed-cycle helium cryostat, which maintained temperature to within 0.1 K at $T \le 100$ K or 0.5 K at $100 < T \le 300$ K. As the valence of samarium in $Sm_{1-x}Y_xS$ exhibited a noticeable temperature hysteresis, the spectra were measured under identical conditions with progressively increasing temperature after cooling the samples to 20 K. The spectra were processed in the VIPER software environment [7].

The EXAFS spectra were processed in accordance with the standard equation

$$\chi(k) = \pm S_0^2 \sum_n \frac{1}{kR_n^2} N_n |f_n(\pi, k)|$$

$$\times \sin[2kR_n + 2\delta_1(k) + \phi_n(\pi, k)] e^{-2\sigma_n^2 k^2}, \quad (1)$$

where $\chi(k)$ is the EXAFS function; N_n is the coordination number; R_n is the average radius of the nth coordination sphere; and σ_n^2 is the standard deviation of the interatomic distance from its average value, referred to as the Debye–Waller factor. The scale factor S_0^2 takes into account multielectron effects. The ± signs apply to the processing of the Sm L_{III} and Y K edges, respectively. The amplitudes $f_n(\pi, k)$ and the backscattering phases $2\delta_1(k) + \phi_n(\pi, k)$ were calculated using the FEFF-8.20 program [8]. As a result of the simulation of

the EXAFS spectra, the coordination numbers, radii, and Debye–Waller factors were obtained for the nearest coordination spheres Sm–S, Sm–Sm, Sm–Y, Y–S, and Y–Sm.

An analysis of the samarium L_{III}-edge XANES spectra was used in order to determine the valence of samarium.

Figure 1 shows the samarium L_{III}-edge XANES spectra of $Sm_{1-x}Y_xS$ measured at $T = 20$ K. All of the test compositions exhibited absorption edge splitting into two maxima shifted by ~7 eV with respect to one another. This is indicative of an intermediate-valence state of samarium, and the average valence of samarium can be determined from the ratio between maximum amplitudes [9]. It is believed that a non-integer valence of samarium is related to partial f-electron delocalization when the $4f$-level position E_0 coincides with the Fermi energy E_F [10]. In this case, the f-electron wavefunction is described by a linear combination of the wavefunctions of $4f^65d^0$ and $4f^55d^1$ states: $\Psi = \alpha\psi(4f^65d^0) + (1 - \alpha)\psi(4f^55d^1)$, where the coefficient $0 \le \alpha \le 1$ characterizes the degree of $4f$-electron localization. The valence of samarium was quantitatively evaluated by simulating the spectral shape using the sum of contributions from Sm^{2+} and Sm^{3+} edges in accordance with the equation [11]

$$I(E) = \sum_{k=1,2} \frac{p(k)\Gamma^2}{\Gamma^2 + (E - E_k)^2}$$

$$+ \sum_{c=1,2} \frac{p(c)}{p(1) + p(2)} \left(\frac{1}{2} + \frac{1}{\pi} \arctan \frac{[E - (E_c + \delta)]}{0.5\Gamma} \right), \quad (2)$$

where Γ is the halfwidth of the Lorentzian that simulates a photoelectron transition from the $2p$ level to the free $5d$ level in the conduction band; $p(1)$, $p(2)$, E_1, and E_2 are the Lorentzian weights and center positions for bivalent and trivalent samarium ions, respectively; E is the x-ray photon energy; and $\delta \sim -1.6$ eV is a small shift characteristic of metallic systems [9]. The Lorentzians describe the photoelectron transition to the $5d$ level, whereas the arctangent adequately represents the character of photoelectron excitation to the region of a continuous spectrum. To simulate experimental broadening, the overall function is convolved with a Gaussian distribution.

The dashed line in Fig. 1 shows the absorption edge spectrum of samarium in $Sm_{0.67}Y_{0.33}S$ at $T = 300$ K. A considerable change in the ratio between maximum amplitudes suggests that the valence of samarium essentially depends on temperature. Figure 2 shows the results of an analysis of XANES spectra. It can be seen in Fig. 2 that a monotonic increase in the valence of samarium with increasing yttrium content was observed at $T = 300$ K. An increase in the temperature from 20 to 300 K also resulted in an increase in the valence; the most dramatic change in the valence from
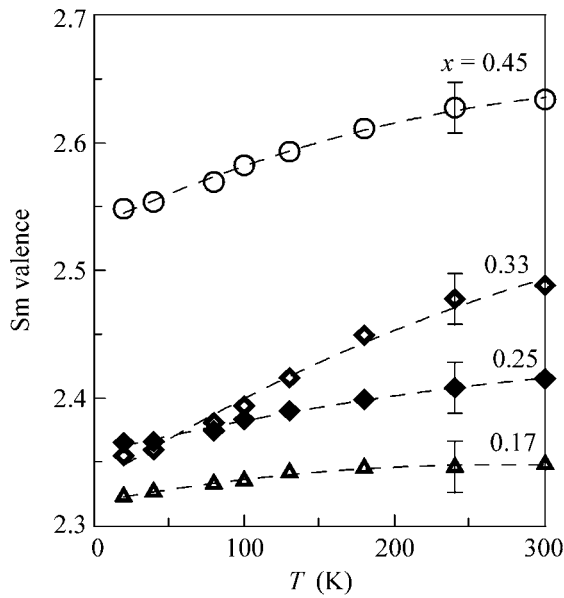
Fig. 2. Temperature dependence of the valence of samarium in samples with various yttrium contents.

Fig. 3. Temperature dependence of the Sm–S and Y–S bond lengths in samples with various yttrium contents.

$v = 2.36$ to $v = 2.49$ was observed in $Sm_{0.67}Y_{0.33}S$. In the other compositions, the valence change was less pronounced and equal to $\delta v = 0.09$, 0.06, or 0.04 at $x = 0.45$, 0.25, or 0.17, respectively.

An analysis of the EXAFS spectra of the same samples showed a monotonic decrease in the Sm–S bond length with both temperature and yttrium content (see Fig. 3). An analogous decrease in interatomic distances was also observed in Sm–Sm and Sm–Y bonds, which are not shown in Fig. 3. This is consistent with the observation of a negative coefficient of thermal expansion [3] because of a decrease in the ionic radius of samarium in accordance with the above-mentioned increase in its valence. In this case, as can be seen in Fig. 3, the Y–S bond length is much shorter than the Sm–S bond lengths in each of the test compositions and almost independent of yttrium content. These data suggest a considerable local deformation in the lattice of SmS upon doping with yttrium, which causes a local reduction of symmetry: indeed, sulfur ions, which are located between samarium and yttrium ions, are shifted from central positions toward Y^{3+} ions by 0.3–0.8 Å depending on x.

Moreover, note that, at $T = 20$ K, the valence of samarium in the composition with $x = 0.33$ is lower than that for $x = 0.25$ (Fig. 2), although the Sm–S bond length in the sample with $x = 0.25$ is much greater (Fig. 3). This suggests a violation of the Vegard law for rare earth compounds in $Sm_{1-x}Y_xS$; this law implies a linear relationship between valence and lattice parameter (interatomic distance) [12]. As the valence of samarium depends on the degree of f-electron delocalization when the $4f$ level and the Fermi level coincide, we
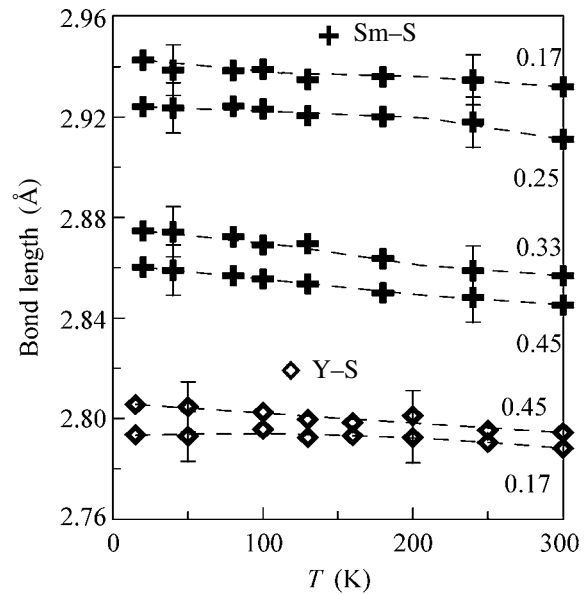
assume that the above violation of the Vegard law is due to the appearance of an additional concentration of $5d$ electrons from Y^{3+}, which shifts the Fermi level in $Sm_{1-x}Y_xS$ toward higher energies. Thus, the effect of doping cannot be reduced to only chemical pressure, because it causes changes in both the local crystal and local electronic structures of SmS.

The local reduction of the SmS lattice symmetry upon yttrium doping can be responsible for the appearance of broadened lines in the spectrum of magnetic excitation [4]. However, this reduction of symmetry, which is directly related to the intermediate-valence state of samarium, can hardly be interpreted as only a systematic change in crystal electric field effects, as suggested by Fishman and Liu [6].

An analysis of EXAFS spectra also allowed us to determine the temperature dependence of the Debye–Waller factors of the Sm–S bond. In x-ray absorption spectroscopy, the Debye–Waller factor, which is equal to the standard deviation of interatomic distance from the average value,

$$\sigma^2 = \sigma_s^2 + \sigma_d^2, \qquad (3)$$

is determined by the temperature-independent contribution σ_s^2, which characterizes the static disorder of atoms, and the dynamic contribution σ_d^2, which characterizes interatomic distance changes due to thermal vibrations. The temperature dependence of the dynamic
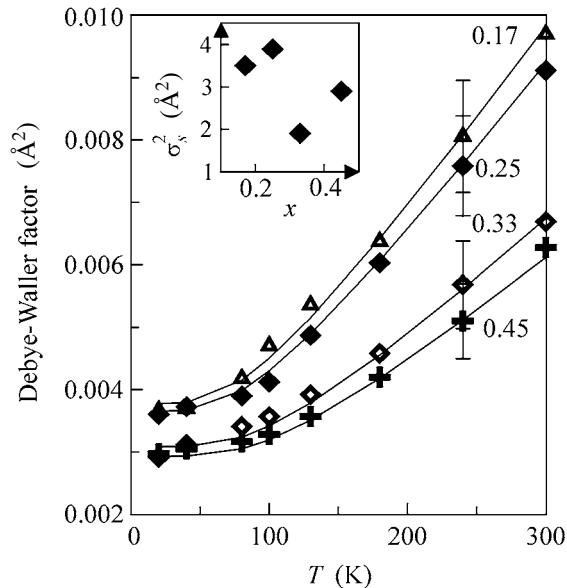
Fig. 4. Temperature dependence of the dynamic contribution σ_d^2 to the Debye–Waller factor for the Sm–S bond. Simulated curves correspond to the Einstein temperatures $\Theta_E = (x = 0.17)\ 243,\ (x = 0.25)\ 251,\ (x = 0.33)\ 297$, and $(x = 0.45)\ 313$ K. The inset shows the dependence of the static contribution σ_s^2 on yttrium content.

Fig. 5. Yttrium-content dependence of the changes in (solid squares) samarium valence $\delta v = v(300\ \text{K}) - v(20\ \text{K})$ and (circles) Sm–S bond length $\delta l = l(20\ \text{K}) - l(300\ \text{K})$ over the temperature range 20–300 K.

contribution can be calculated within the framework of the Einstein model [13]:

$$\sigma_d^2 = \frac{\hbar}{2\omega\mu}\coth\frac{\Theta_E}{2T}, \qquad (4)$$

where ω is the frequency of longitudinal vibrations of the bond, μ is the reduced mass of the atomic pair; and $\Theta_E = \hbar\omega/k_B$ is the Einstein temperature.

Figure 4 shows the experimental results together with simulated curves. It can be seen that the rigidity of the Sm–S bond, which is characterized by the Einstein temperature, increases monotonically with yttrium content; this is consistent with the above decrease in the bond length. Simultaneously, it was found that the composition with $x = 0.33$ exhibited minimum local static distortions in the crystal lattice, which are characterized by a minimum value of the static Debye–Waller factor of the Sm–S bond (Fig. 4, inset). This circumstance suggests the greatest degree of ordering in the Sm$_{1-x}$Y$_x$S lattice at the yttrium concentration $x = 0.33$. Indeed, for a lattice of the NaCl type, the number of the nearest neighbors in the samarium sublattice is equal to 12, and the local environments of each of the samarium ions are practically identical and consist of eight samarium ions and four yttrium ions at $x = 0.33$. Naturally, the simulation of lattice distortions upon doping dem-
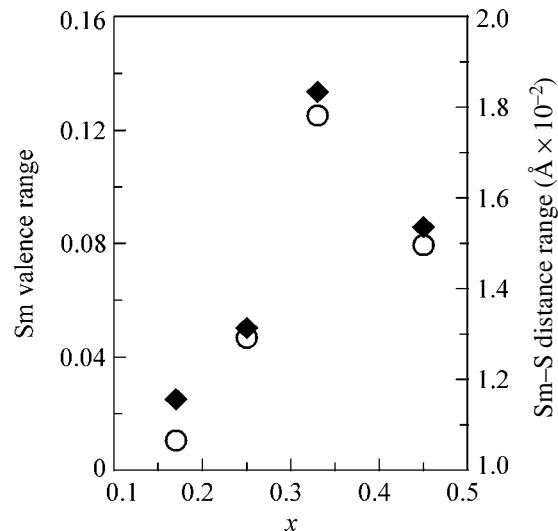
onstrated that this composition corresponds to a minimum degree of local deformation.

A correlation between the peculiarities of the local crystal and local electronic structures of an intermediate-valence state in Sm$_{1-x}$Y$_x$S manifests itself as absolutely identical changes in the valence state of samarium $\delta v = v(300\ \text{K}) - v(20\ \text{K})$ and in the Sm–S bond length $\delta l = l(20\ \text{K}) - l(300\ \text{K})$ as functions of yttrium content over the temperature range 20–300 K, which are shown in Fig. 5. Note that the above changes exhibit a maximum in the sample with $x = 0.33$, which has the most ordered lattice on a local level.

The experimental results allowed us to propose a model for the relation of the valence state of samarium with the local peculiarities of the Sm$_{1-x}$Y$_x$S lattice in order to determine the main characteristics of the intermediate-valence state. Because the valence of samarium depends on the degree of overlapping of 4f states with free states near the Fermi level, it will depend on the depth and width of the 4f level. In the most ordered lattice with $x = 0.33$, where the valence of each of the Sm ions is practically the same because of identical local environments, the 4f-level halfwidth Γ_f reaches a minimum and coincides with the 4f-level halfwidth of an individual ion. In this case, the broadening of the 4f level is homogeneous and described by the Lorentz function. With a deviation from this concentration, each of the samarium ions exhibits a somewhat different local environment. This results in an inhomogeneous integral broadening of the 4f level, which is described by the Gauss function. As a result, the same "smearing" k_BT of the Fermi level E_F, as the temperature was increased from 20 to 300 K, caused different changes in the degree of its overlapping with the 4f level depend-

ing on the depth $\Delta E = E_F - E_0$ and the halfwidth Γ_f of the 4f level. For a minimum halfwidth of the 4f level ($x = 0.33$), the change in the degree of overlapping reached a maximum; thus, a maximum change in the valence of samarium with temperature took place in the composition with $x = 0.33$ (see Fig. 5). Minimum changes in the valence correspond to the compositions with $x = 0.17$ and 0.25, in which local lattice distortions reached a maximum.

Based on the proposed model and the experimentally found temperature dependence of the valence of samarium, we evaluated important characteristics of the intermediate-valence state such as the energy depth ΔE and the halfwidth Γ_f of the 4f level and summarized them in the table. The resulting values of the width of the 4f level are consistent with the estimated width of the hybridized f band $10^{-2} \leq \Gamma_f \leq 10^{-1}$ eV, which was cited by Varma [10], as well as with more recent theoretical estimations (e.g., see [14]), in terms of the order of magnitude.

We experimentally found that the effect of doping on an intermediate-valence state in $Sm_{1-x}Y_xS$ cannot be reduced to only chemical pressure generation. A change in the local environment parameters of the samarium ion results in a noticeable rearrangement of its electronic structure. The replacement of samarium ions with yttrium, on the one hand, causes a local symmetry breakdown in the SmS lattice and, on the other hand, affects the valence of samarium to convert it into an intermediate-valence state, which additionally contributes to the local lattice deformation. The electron doping caused by the replacement of bivalent samarium ions with trivalent yttrium ions shifts the Fermi level toward higher energies to result in a violation of the Vegard law. The temperature dependence of the valence of samarium is responsible for an anomalous decrease in the lengths of interatomic bonds with temperature to cause an integrated negative coefficient of thermal expansion. A combination of XANES and EXAFS techniques, which provides an opportunity to simultaneously analyze temperature changes in the valence and local structural distortions, allows us to evaluate important parameters of the intermediate-valence state such as the energy width of the 4f level and its position with respect to the Fermi level.

Energy depth $\Delta E = E_F - E_0$ and halfwidth Γ_f of the Sm 4f level in $Sm_{1-x}Y_xS$ for samples with various yttrium contents at $T = 20$ K

	$x = 0.17$	$x = 0.25$	$x = 0.33$	$x = 0.45$
Γ_f, eV	0.37	0.22	0.09	0.13
ΔE, eV	0.12	0.05	0.02	−0.01

REFERENCES

1. D. I. Khomskiǐ, Usp. Fiz. Nauk **129**, 443 (1979) [Sov. Phys. Usp. **22**, 879 (1979)].
2. L. D. Finkel'shteǐn, N. N. Efremova, N. I. Lobachevskaya, et al., Fiz. Tverd. Tela (Leningrad) **18**, 3117 (1976) [Sov. Phys. Solid State **18**, 1818 (1976)].
3. K. Iwasa, T. Tokuyama, M. Kohgi, et al., Physica B (Amsterdam) **359–361**, 148 (2005).
4. P. A. Alekseev, J.-M. Mignot, A. Ochiai, et al., Phys. Rev. B **65**, 153201 (2002).
5. K. A. Kikoin and A. S. Mishchenko, J. Phys.: Condens. Matter **7**, 307 (1995).
6. R. S. Fishman and S. H. Liu, Phys. Rev. Lett. **89**, 247203 (2002).
7. K. V. Klementev, J. Phys. D: Appl. Phys. **34**, 209 (2001).
8. A. L. Ankudinov, B. Ravel, J. J. Rehr, and S. D. Conradson, Phys. Rev. B **58**, 7565 (1998).
9. J. Röhler, J. Magn. Magn. Mater. **47–48**, 175 (1985).
10. C. M. Varma, Rev. Mod. Phys. **48**, 219 (1976).
11. P. P. Deen, D. Braithwaite, N. Kernavanois, et al., Phys. Rev. B **71**, 245118 (2005).
12. A. Jayaraman, P. D. Dernier, and L. D. Longinotti, Phys. Rev. B **11**, 2783 (1975).
13. E. Sevillano, H. Meuth, and J. J. Rehr, Phys. Rev. B **20**, 4908 (1979).
14. V. N. Antonov, B. N. Harmon, and A. N. Yaresko, Phys. Rev. B **66**, 165208 (2002).

Translated by V. Makhlyarchuk